Third-generation sensors for night vision

P. NORTON*

IR Vision, 2922 Paseo del Refugio, Santa Barbara, CA 93105, USA

Third generation sensors are under development to enhance capabilities for target detection and identification, threat warning, and 3D imaging. Distinct programs for both cooled HgCdTe and uncooled microbolometer devices are part of this thrust. This paper will describe the technology for HgCdTe two-colour, high-definition imaging sensors and threat warning devices, avalanche photodiode arrays for 3D imaging, and the supporting technology being developed to enhance the readouts that support these devices. Uncooled detector initiatives will also be described to reduce pixel size in conjunction with the production of 480×640 arrays. Finally, efforts are also beginning to move both photon and thermal detectors closer to radiative-limited performance while simultaneously reducing the cooling requirements for photon detectors.

1. Introduction

Infrared imaging development [1] began in the 1950's after it was established that objects retained thermal contrast around the clock [2], Figs. 1, 2, and 3. First generation imagers utilized scanned single-element detectors and linear arrays. Early systems employed InSb and PbSe in the MWIR region (3–5 μm), and Ge:Hg in the LWIR region (8–14 μm). The first forward-looking infrared (FLIR) system based upon Ge:Hg provided excellent imagery for B-52 and other aircraft but required a two-stage cooler to operate the detector array at approximately 25 K. Two-stage coolers had limited lifetime and system maintenance was an issue when consideration was given to fielding infrared imagers in tank fleets having thousands of vehicles.

Photoconductive HgCdTe provided a way to solve the cooler lifetime problem. HgCdTe, being an intrinsic narrow bandgap material could operate in the 8–12 μm LWIR band at 80 K, a temperature readily reached with a single stage cooling system. Like the B-52 Ge:Hg FLIR, the system was a parallel scanner. Production of these first-generation systems began in the late 1970s. Army units were known as "Common Modules" and arrays with 60, 120, and 180 elements were built for a variety of platforms. The Air Force and Navy used minor variations of the basic array in 160 and 180 element configurations for navigation, tracking, and targeting.

The British successfully fielded FLIRs with similar sensitivity using serial-parallel scanners and photoconductive HgCdTe detectors with fewer elements, but with some analogue time-delay and integration (TDI) capabilities through a very clever method involving synchronizing the scan speed and the ambipolar drift velocity in an elongated detective element.

Second generation infrared imaging began in the late 1980's with photovoltaic HgCdTe arrays in a parallel-scanned system, but with TDI of four elements in each row. These are arrays of 240×4 or 480×4, depending upon which system they went into. The combination of photovoltaic operation with reduced $1/f$ noise and a greater number of detector elements to sample the scene significantly improved FLIR imagery while retaining much of the common system housing and optics.

In the early 1990's, fully two-dimensional second-generation arrays provided a means for staring sensor systems to begin production. HgCdTe LWIR sensors in 64×64 and 256×256 formats were most commonly used. InSb in 480×640 format became available a few years later for MWIR system use. By the late 1990's, array sizes approaching 2k×2k were in prototype testing. Figure 4 shows the history of second generation staring array detector development and the beginning of third-generation, two-colour array demonstrations.

The new millennium began a process of defining and developing third-generation infrared sensors. The definition itself is the outcome of local opinions and not based on any objective criteria. However, it is widely, if not universally, held that third-generation sensors are not simply very large arrays with the same features as second-generation sensors. That would imply a threshold for some key capability as array size expanded, whereas none is known.

The U.S. Army defined third-generation sensors [3] for it's own purposes several years ago as:
- high-performance, large-format cooled imagers with two- or three-colour bands,
- medium- to high-performance uncooled imagers,
- very low cost, expendable uncooled imagers.

* e-mail: p.norton@verizon.net

Fig. 1. A "portable" infrared radiometer used to measure infrared scene profiles at Syracuse University in the late 1950's. John Stannard, left, was an undergraduate at the time of this picture. He later received his PhD under Professor Henry Levinstein. The identity of the student on the right is not known.

This definition is generally fluid – for example a cooled sensor may be considered third-generation if it combined a passive-mode for conventional infrared search together with an active-mode capability for acquiring 3D imagery in conjunction with a pulsed laser.

This paper will focus chiefly on the first topic of high performance cooled sensors with capabilities beyond single-colour 2D imaging, and briefly with establishing high

Fig. 3. Background line scans at 4.75 μm of a campus scene for a series of times between 18:08 and 19:21. In the scene, sky was above, followed by smoke, smokestack, house, iron pipes, and concrete steps. Of significance was the persistence of the step's features over time under most weather conditions.

performance large format uncooled imagers to replace many first- and second-generation systems in less stressing applications. To begin with we first review the challenges to be addressed in future infrared focal plane technology development, followed by some examples of the programs underway to realize these goals.

Fig. 2. Spectral radiometer used for early measurements of infrared terrain signatures.

Fig. 4. Detector array pixel count has paralleled the exponential growth of silicon dynamic random access memory (DRAM) bit capacity. CCDs with close to 100 M pixels offer the largest formats. In the infrared, 4 M pixel arrays are now available for astronomy applications.

2. Challenges

Many challenges are faced by the infrared community in developing the technology needed to field high-performance third-generation cooled imagers. These devices are expected to provide high spatial and temporal resolution simultaneously in two- to three-bands. Performance has to be close to the theoretical limit, dominated by the limits of photon noise. We consider here the principal challenges:

- pixel and chip size issues combined with two- and three-colour formats,
- high frame rate operation,
- temperature cycling fatigue,
- dynamic range and sensitivity constraints,
- more precise non-uniformity correction,
- higher operating temperature.

These challenges are now very briefly listed – more detailed discussions have been given previously [3,4].

Pixel and chip size issues in association with two- and three-colour imager formats
Readout wafers are processed in standard commercial foundries and can be constrained in size by the die-size limits of the photolithography step-and-repeat printers. Other reasons to develop small pixels are critical considerations of cost, weight, and spatial resolution.

High frame rate operation
Higher frame rates pose significant issues with respect to power dissipation.

Temperature cycling fatigue
Very large focal plane arrays may exceed the limits of hybrid reliability engineered into current cooled structures.

Dynamic range and sensitivity constraints
A goal of third-generation imagers is to achieve an order of magnitude or more sensitivity improvement, corresponding to about 1 mK *NEΔT*. Considering the relative change in photon flux from a 1 mK change in a 300 K scene over the LWIR region, this implies a sensitivity of 1.8×10^{-5} – requiring a charge storage capacity of 6×10^9 e$^-$ based only on counting statistics. Also note that this corresponds to a dynamic range of 5.5×10^4 or 95 db, and saturation will occur at a scene temperature of only 355 K even with such a large dynamic range.

Non-uniformity correction
Non-uniformity correction of pixel responsivity must be improved an order of magnitude to 0.004% as the sensitivity drops to 2.5 mK.

Higher operating temperature
Power can be saved, and cooler efficiency and cooler lifetime improved if focal planes can be operated at elevated temperatures.

3. Development effort examples

This section will review some of the ongoing efforts underway to demonstrate third-generation infrared sensors, and to prepare the technology for production.

3.1. Two colour sensors

Two colour manufacturing programs are under way sponsored by the Navy and by the Army. In the former case, the two bands are in the medium wavelength region (MWIR) and the application is for threat warning. This program has been described by Waterman [5].

Recently, the Army began a manufacturing technology program to develop large format (1280×720 pixels), two-colour sensor with a combination of MWIR and LWIR sensitivity [4]. The sensor has both colours collocated in a 20-µm pixel. This sensor is being developed to greatly extend the range at which targets can be detected and identified. US Army rules of engagement now require identification prior to attack. Since deployment of first and second generation sensors, there has been a gradual proliferation of thermal imaging technology world-wide. Third-generation sensors are intended to ensure that US Army forces maintain a technological advantage in night operations over any opposing force.

The two-colour sensor is used to first detect an object, and then to identify it. In the detection mode, the optical system provides a wide field of view (WFOV–*f*/2.5) to maintain robust situational awareness [6]. For detection, long wave-length infrared (LWIR) provides superior range under most Army fighting conditions. Medium wavelength infrared (MWIR) offers higher spatial resolution sensing, and a significant advantage for long-range identification when used with telephoto optics (NFOV–*f*/6).

Figure 5 compares the relative detection and identification ranges modelled for the third-generation cooled imager. Range criteria is the standard 70% probability of detection or identification as modelled by NVESD's NVTherm program. Note that the identification range in the MWIR NFOV 3rd generation imager is almost 70% of the LWIR detection range.

Cost is a direct function of the chip size since the number of detector and readout die per wafer is inversely proportion to the chip area. Chip size in turn is set by the array format and pixel size. Third-generation imager formats for Army applications are anticipated to be in a high-definition TV 16×9 layout, compatible with future display standards, and reflecting the soldier's preference for wide field of view. An example of such a format is 1280×720 pixels. For a 30-µm pixel this format yields a die size greater than 1.5×0.85 inch (22×38 mm). This will yield only a few die per wafer, and will also require the development of a new generation of dewar-cooler assemblies to accommodate these large dimensions. A pixel size of 20 µm results in a cost saving of more than 2×, and allows the use of existing dewar designs.
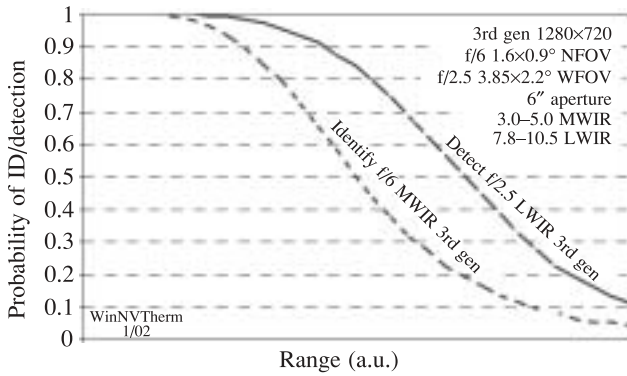
Fig. 5. Comparison of the detection and identification range of a third-generation imager in a 1280×720 format with 20-μm pixels.

Pixel size is the most important factor for achieving affordable third-generation systems. Two types of two-colour pixels have been demonstrated. Simultaneous two-colour pixels have two indium bump connections per pixel to allow readout of both colour bands at the same time. Figure 6 shows an example of a sequential two-colour approach that requires only one indium bump per pixel, but requires the readout circuit to alternate bias polarities multiple times during each frame. Both the simultaneous and sequential approaches leave very little area available for the indium bump(s) as the pixel size is made smaller, as illustrated in Fig. 7. Advanced etching technology is one of the materials technologies being developed in order to meet the challenge of shrinking the pixel size to 20 μm [4].

A major consideration in selecting a format was the packaging requirements. Infrared sensors must be packaged in a vacuum enclosure and mated with a mechanical cooler for operation. Overall array size was therefore limited to approximately one inch so that it would fit in an existing SADA dewar design. Figure 8 illustrates the pixel size/format/field-of-view trade within the design size constraints of the SADA dewar.

A goal of third-generation imagers is to achieve a significant improvement in detection and ID range over second-generation systems. Range improvement comes from

Fig. 7. SEM of a 20-μm sequential two-colour pixel structure.

Fig. 8. Maximum array horizontal format is determined by the pixel size and the chip size limit that will fit in an existing SADA dewar design for production commonality. For a 20-μm pixel and a 1.6°FOV, the horizontal pixel count limit is 1280. A costly development program would be necessary to develop a new, larger dewar.

Fig. 6. Illustration of a sequential two-color pixel structure in cross section. Sequential two-colour FPAs have only one indium bump per pixel, helping to reduce pixel size.
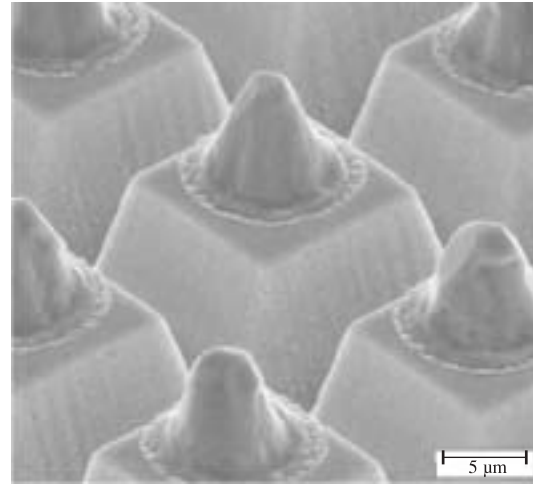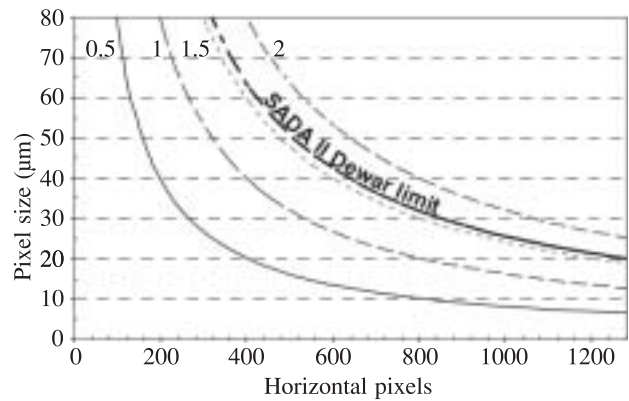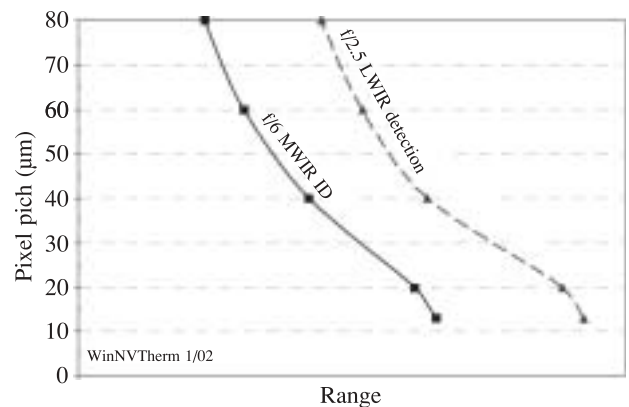

Fig. 9. Range improves as the pixel size is reduced until a limit in optical blur is reached. In the examples above, the blur circle for the MWIR and LWIR cases are comparable since the f/number has been adjusted accordingly. D^* and integration time have been held constant in this example.

higher pixel count, and to a lesser extent from improved sensitivity. Figure 9 shows relative ID and detection range vs pixel size in the MWIR and LWIR respectively. Sensitivity (D^* and integration time) have been held constant, and the format was varied to keep the field-of-view constant.

Sensitivity has less effect than pixel size for clear atmospheric conditions, as illustrated in Fig. 10. Note that here the sensitivity is varied by an order of magnitude, corresponding to two orders of magnitude increase in integration time. Only a modest increase in range is seen for this dramatic change in signal-to-noise ratio. In degraded atmospheric conditions, however, improved sensitivity plays a larger role because the signal is weaker. This is illustrated in Fig. 10 by the curve showing range under conditions of reduced atmospheric transmission.

Dynamic range of the imager output must be considered from the perspective of the quantum efficiency and the effective charge storage capacity in the pixel unit cell of the readout. Quantum efficiency and charge storage capacity determine the integration time for a particular flux rate. As increasing number of quanta are averaged, the signal-to-noise ratio improves as the square root of the count. Higher accuracy analogue-to-digital (A/D) converters are therefore required to cope with the increased dynamic range between the noise and signal levels.

System interface considerations lead to some interesting challenges and dilemmas. Imaging systems typically specify a noise floor from the readout on the order of 300 μV. This is because system users do not want to encounter sensor signal levels below the system noise level. With readouts built at commercial silicon foundries now having submicrometer design rules, the maximum bias voltage applied to the readout is limited to a few volts – this trend has been downward from 5 V in the past decade as design rules have shrunk. Output swing voltages can only be a fraction of the maximum applied voltage, on the order of 3 V or less.
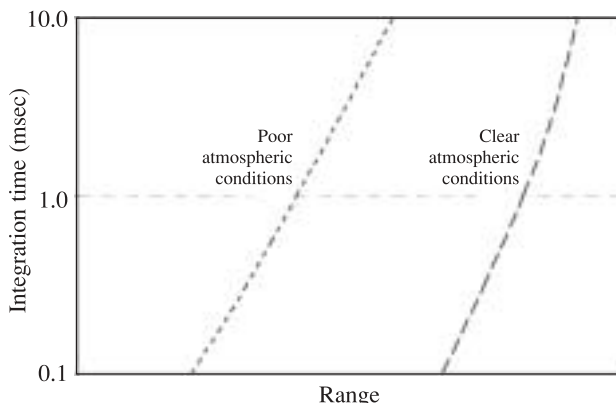
This means that the analogue dynamic range limit of a readout is about 10000–80 db in power – or less. Present readouts almost approach this constraining factor with 70–75 db achieved in good designs. In order to significantly improve sensitivity, the noise floor will have to be reduced.

If sufficiently low readout noise could be achieved, and the readout could digitize on chip to a level of 15–16 bits, the data could come off digitally and the system noise floor would not be an issue. Such developments may allow incremental improvement in third-generation imagers in the future. The third section will describe another development effort to address readout and other on-focal-plane signal processing issues for third-generation sensors.

Very significant progress is being made on programs to develop the sensors described in this section. Raytheon has already demonstrated [7] working two-colour MWIR/LWIR arrays with 20-μm pixels in a 480×640 format with high response operability ≥ 99%. $NE\Delta T$ values less than 25 mK at f/5 have been demonstrated for both bands. The LWIR cut off wavelength was approximately 10.5 μm. The Raytheon design uses a single indium bump per pixel, as illustrated in Fig. 6. To accommodate this, the detector bias is reversed multiple times per frame, giving nearly simultaneous integration. In fact, because the MWIR flux is much less than the LWIR flux, the MWIR integration time is overall longer to provide about the same $NE\Delta T$ values.

An example of imagery from one of over 70 arrays in the 480×640 format built by Raytheon in the first phase of the program is shown in Fig. 11. Raytheon plans to demonstrate a full 720×1280 format later in 2005.

DRS is working on another contract to develop these large format, two-colour arrays [8]. They use an alternative detector structure with two contacts per pixel. In their most recent publication they have been able to achieve 25-μm pixel pitch and are working towards 20-μm pixels.

Rockwell Scientific has a third contract for development of large third-generation sensors.

3.2. Avalanche photodiodes

Looking into the prospects for extending the identification range further, and in the presence of partial obscuration or camouflage netting, short wavelength infrared (SWIR) sensors capable of imaging reflected laser pulses are being investigated. The SWIR spectral region at 1.5 μm and beyond is of specific interest because it poses less risk for eye damage from lasers.

Two types of HgCdTe avalanche photodiodes (APDs) are being investigated for such applications, in addition to classic APDs using InGaAs. The first type of HgCdTe APD [9] relies on a novelty in the energy band structure of HgCdTe with a bandgap of approximately 0.82 eV. Here the bandgap energy becomes equal to the energy separation between the top of the valence band and the split-off light-hole band below it. The device structure, band structure, and avalanche mode is illustrated in Fig. 12. This de-
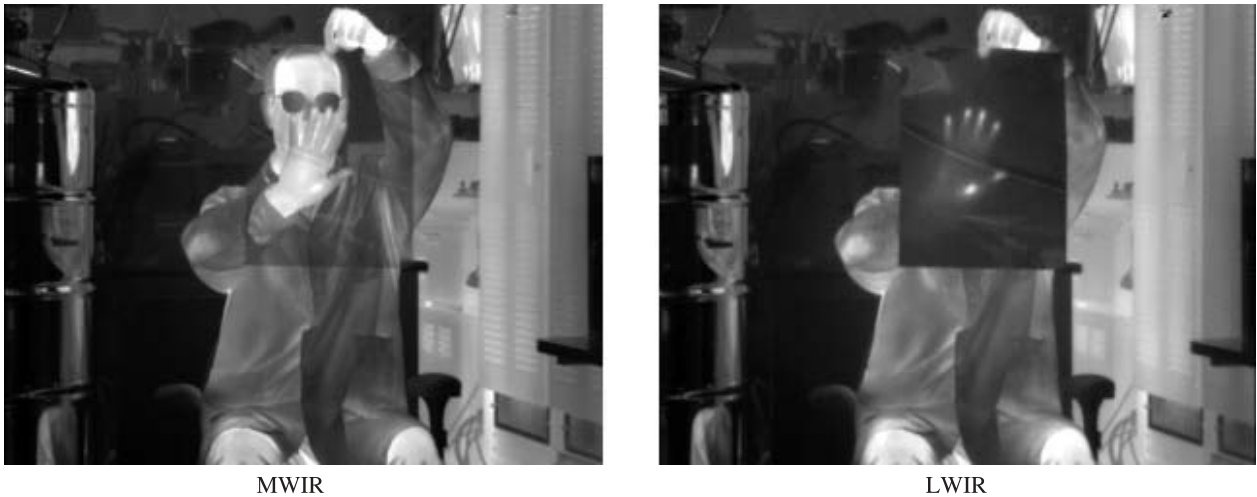

Fig. 10. Range in a clear atmosphere improves only modestly with increased sensitivity. The case modeled here has a 20-μm pixel, a fixed D^*, and variable integration time. The 100× range of integration time corresponds to a 10× range in signal-to-noise. Improvement is more dramatic in the case of lower atmospheric transmission that results in a reduced target signal.

MWIR   LWIR

Fig. 11. Example of imagery obtained at 78 K for an Army 640×480 M/LWIR FPA (#7586704) at *f*/5 field of view and 30 Hz frame rate. The subject is holding a thin piece of plastic which transmits in the MWIR band but absorbs in the LWIR band. Photo courtesy of W. Radford of Raytheon Vision Systems.

vice yields hole avalanche conditions that are much more favourable than electron avalanche. Such conditions result in gain with low noise. A major benefit of this approach is operation with little or no cooling required.

An alternative HgCdTe APD approach is being developed by DRS [10] and BAE Systems Infrared in England [11] using electron avalanche. This approach leverages the unique device structure developed for their standard photodiodes, as shown in Fig. 13. BAE Systems Infrared, refers to this type of diode as a loophole [12], while DRS calls it a high-density vertically-integrated photodiode (HDVIP) [13]. The radial electric field surrounding the central contact leads to a concentrated electric field in that region that can ballistically accelerate low-mass electrons to impact ionize in narrow bandgap HgCdTe. In this case the avalanche conditions greatly favours electrons over holes, again giving high gain with low excess noise. However, because this approach uses narrower bandgap material in the avalanche process the device must be cryogenically cooled. Efforts are underway to determine the largest bandgap at which this device will successfully work, corresponding to the least amount of cooling required. A significant advan-

tage of this approach occurs for applications in which both a thermal detector and an avalanche detector are desired in a single array. At low bias the device can operate as a conventional detector and can have state-of-the-art sensitivity in the MWIR spectral region. At higher bias it can then be made to operate with high gain for 3D range imaging. Such a sensor may be realized in the near future due to the readout technology being developed as described in the following section.

Electron-avalanche APDs have also recently been explored using standard HgCdTe MWIR mesa diodes [14]. Gains up to a factor of 100 have been obtained with this approach.

3.3. Structures for advanced readouts and other on-focal-plane signal processing functionality

Visible and infrared sensors for third-generation imaging systems will provide a variety of new capabilities. These sensors are being designed to enhance the ability to identify targets at long range, overcome camouflage, find targets in cluttered backgrounds, and counter laser threats. The task
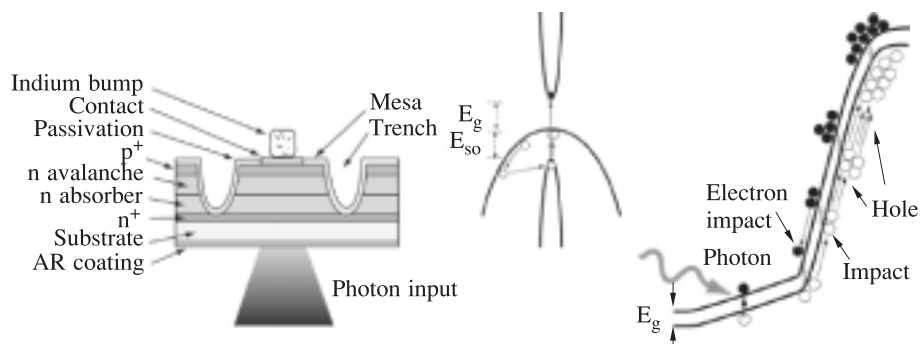

Fig. 12. Hole avalanche device structure (left), energy band diagram (center), and hole avalanche mechanism (right). The bandgap of the avalanche region is tuned to the resonance condition depicted in the center figure in which the bandgap and the split-off valence band are equi-distant from the top of the heavy-hole valence band.
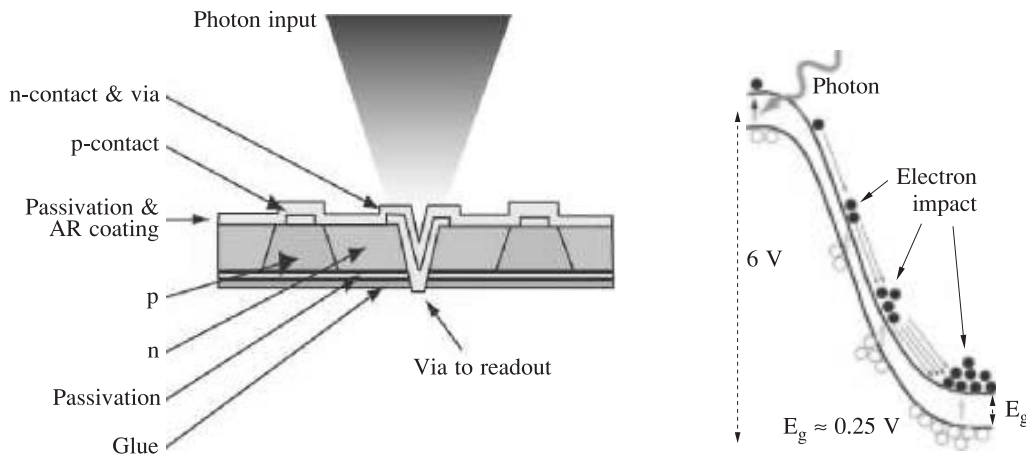
Fig. 13. Electron avalanche structure consists of central n-type region surrounded by p-type material.

of amplifying, conditioning, pre-processing, and digitizing the signals from these sensors requires a considerable advance in sensor readout technology. Current readout technology is based upon CMOS circuitry that has benefited from the dramatic and continuing progress in miniaturizing circuit dimensions.

Sensors that are being developed for active imaging systems, such as LADAR, require signal acquisition with precise time-stamped data so that the target range is determined for 3D image construction. This functionality will not fit in small unit cells along with a conventional video signal input circuit for sensors that need to combine both passive and active imagining. The vertically-integrated sensor array (VISA) program will provide additional layers for circuit implementation of dual mode readouts [15,16].

VISA will provide an opportunity to significantly increase both the charge storage capacity and the dynamic range. This will permit LWIR focal planes to improve the sensitivity by a factor of ten.

The VISA program offers the possibility to move most, or all of the camera circuit board functions into layers of circuits under the focal plane, allowing camera engines to be shrunk to dimensions comparable to today's sensor chips.

Finally, the VISA program is motivated to increase the dynamic range very significantly – to ≥ 20 bits (≥ 120 dB), from the current limits of 10–12 bits for visible imagers and 14 bits (80 dB) for infrared sensors.

Figure 14 illustrates the VISA technology concept. A detector array is hybrid bump-bonded to a silicon layer that provides input circuits appropriate for the sensor. Monolithic implementations combining the input and the sensor especially feasible with silicon sensors are not precluded. The input circuit layer is thinned and vias are etched and metalized in order make pixel-level interconnects to the second layer of silicon circuits. Such a layer may provide, for example, analogue non-uniformity correction, large capacitance for charge storage, or threshold, timing, and latching circuits that may be needed in a LADAR application. The second layer is also thinned and pixel-level interconnects are provided to the circuitry on a third level. Third-level circuits

may include colour processing functions following non-uniformity correction in the second level. The final level (fourth in Fig. 14) in most cases is anticipated to be used for converting the analogue signals to digital format. This will allow for significant expansion of the dynamic range from approximately 14 bits to 20 bits or more.

The VISA program utilizes reactive plasma etching to produce vias that connect circuitry on the surface of a thinned wafer through to circuitry on another wafer below it. Shown in the scanning electron micrograph (SEM) images in Fig. 15 is an example of an etched via produced for the program [17]. VISA prime contractors have each teamed with an integrated circuit technology partner to develop this technology for the program. This example has been demonstrated for a full 256×256 format array – 65,536 connections in all.
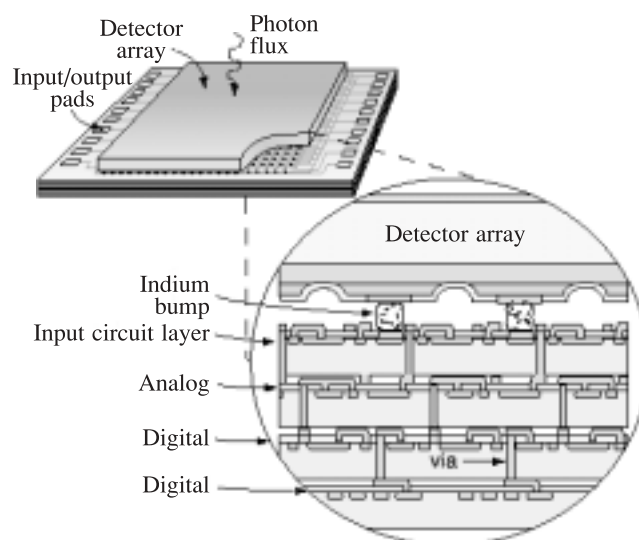

Fig. 14. Multiple layers of readout circuits can be embedded underneath a detector array as shown in this diagram that illustrates four such layers. Each layer is fabricated in a silicon foundry, tested, and then thinned and glued over the layer below. Small vias are etched and metallized to interconnect the circuits at the pixel level.
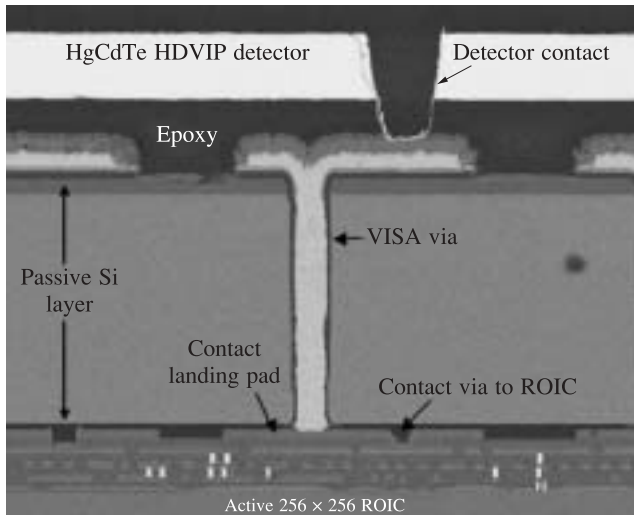
Fig. 15. Via connection demonstration in which contact is made from a HDVIP detector to a readout through a thinned wafer.

The performance impact of VISA is quite significant. It will allow the use of smaller and multi-colour detectors without compromising storage capacity. Signal-to-noise ratios will increase for single-colour and multi-colour focal plane arrays. Low power A/Ds can be integrated in the focal plane stack with extremely wide dynamic range and frame rates as well as physically compact signal processing.

Moving camera circuitry onto the focal plane will reduce electrical power and weight, although at a penalty in cooler power. Massively parallel A/D circuits operating at the pixel level can reduce power because they operate at relatively slow clock rates – once per frame, rather than at very high rates that must be fed by wide-bandwidth output amplifiers driving shielded cables to external circuits.

3.4. Uncooled detectors

Third-generation uncooled sensors are making a transition to production with two principal features – large 480×640 formats, and small 25-μm pixels. These sensors are anticipated to replace many existing first- and second-generation sensors for shorter range imaging and for routine night operations such as vehicle driving. Small pixel development has been a critical issue for reducing the weight and cost, especially as it impacts the optical components of the system.

The status of these developments has been documented by suppliers [18–22], and the objectives of the work by a recent Army perspective [23]. Generally, 25-μm pixel microbolometers are now achieving sensitivities comparable to those common for 50-μm pixel devices of a few years ago. Table 1 summarizes results from recent conference papers [18–22,24]. All of the devices listed in Table 1 are microbolometers based upon vanadium oxide (VO$_x$) thermistors with the exception of Mitsubishi which uses a series of p-n silicon junctions made with silicon-on-insulator (SOI) technology. Table 1 includes a "figure of merit" (*FoM*) as proposed by Kohin and Butler [25], namely

$$FoM = NE\Delta T \times \tau.$$

The FoM, as defined, means that a small number is better than a large one. Also, this *FoM* does not take into account complex issues that concern pixel dimension scaling. To adjust for these, an estimate to correct for these issues can be approximated by $A^2/25^2$, where A is the pixel area in μm. This has been used for the one case in Table 1 where the pixel size differed from 25 μm.

Uncooled detectors in large formats with small pixels are on their way into production. This development will save considerable cost in deployment and maintenance over the life-cycle of these systems, since coolers will not be a necessary and expensive acquisition cost or replacement/repair issue. In parallel, even smaller pixel development is underway.

3.5. Reaching for performance limits

The next focus of the transition to third-generation sensors is to push the performance to approach the theoretical limit at uncooled, or minimally-cooled temperatures for both thermal and photon devices. Work in these tasks has not fully begun, but the issues have been reviewed [26].

Thermal detectors are not currently limited by fundamental parameters such as thermal conductivity or mass, but rather by excess noise contributions from system noise and 1/*f* noise. Improvements of between 3–15× greater sensitivity should be possible just by minimizing these factors. To do this, materials with lower inherent 1/*f* noise characteristics may be needed, along with higher temperature coefficient of resistance to help make detector noise more dominant. Beyond that, further reduction in the properties

Table 1. Comparison of small pixel performance for recently published data on 480×640 format uncooled imagers. The data all assume *f*/1 optics and 30 Hz frame rate.

	BAE Systems	DRS	InfraredVision	Mitsubishi	RVS
Pixel size (μm)	28	25	25	25	25
NEΔT (mK)	< 35	< 50	< 40	< 40	< 35
Time constant (ms)	< 12	< 20	< 20	24	< 12
Figure of merit (ms mK)	527[25]	1000	800	960	420

of fundamental parameters will be needed to reduce $NE\Delta T$ to the thermal fluctuation limit.

Raising the operating temperature of photon detectors while maintaining detector sensitivity and fast response time is another objective. Approaches to this problem have been proposed that involve the application of electrical bias to the device in order to electronically mimic the cooled state of the material. Attempts to achieve this condition have been partially successful, but have been accompanied by excess $1/f$ noise.

Even modest improvements in operating temperature can be important for certain applications of MWIR detectors. Large production potential exists for these devices in threat warning applications for commercial aircraft and for military ground vehicles. Being able to operate with thermal-electric cooling could reduce operational costs compared with those associated with mechanical coolers so that these applications become practical.

Acknowledgements

References

1. L.M. Biberman and R.L. Sendall, "Introduction: A brief history of imaging devices for night vision", in *Electro-Optical Imaging: System Performance and Modelling*, edited by L.M. Biberman, SPIE Press, Bellingham, 2000.

2. Among the early experiments to evaluate the possibility of imaging in the infrared, measurements were carried out at Syracuse University by Professors William R. Frederickson and Nathan Ginsburg, with Roy Paulson and Don Stierwalt as the research associates, and students John Stannard, E. Ellis, E. Hall, and M. MacDonald. The PbTe detector used for the measurements was fabricated by Professor Henry Levinstein. The contracts were sponsored by the Wright Patterson Air Force Base (AF 33(616)–5034), monitored by Neil Beardsley, and by the Air Force Cambridge Research Center (AF 19(604)–3908). The single-element PbTe detector was line-scanned at intervals throughout the day and night. Results showed that the scene retained contrast at all times.

3. P. Norton, J. Campbell III, S. Horn, and D. Reago, "Third-generation infrared imagers", *Proc. SPIE* **4130**, 226–236 (2000).

4. S. Horn, P. Norton, T. Cincotta, A.J. Stoltz, Jr., J.D. Benson, P. Perconti, and J. Campbell III, "Challenges for third-generation cooled imagers", *Proc. SPIE* **5074**, 44–51 (2003).

5. J.R. Waterman, M.R. Kruer, J.M. Schuler, D.A. Scribner, and P.R. Warren, "Multicolour focal plane technology for Navy applications", presented orally at *Infrared Technology and Applications XXVIII*, Seattle, WA, July 2002.

6. It should be noted that the third-generation imager will operate as an on-the-move wide area step-scanner with automated ATR versus second-generation systems that rely on manual target searching. This allows the overall narrower field of view for the third-generation imager.

7. W.A. Radford, E.A. Patten, D.F. King, G.K. Pierce, J. Vodicka, P. Goetz, G. Venzor, E.P. Smith, R. Graham, S.M. Johnson, J. Roth, B. Nosho, and J. Jensen, "Third generation FPA development status at Raytheon Vision Systems", *Proc. SPIE* **5783**, 325–330 (2005).

8. P.D. Dreiske, "Development of two-colour focal-plane arrays based on HDVIP", *Proc. SPIE* **5783**, 325–330 (2005).

9. M.D. Jack, J.F. Asbrock, C. Anderson, S.L. Bailey, G. Chapman, E. Gordon, P.E. Herning, M.A. Kalisher, K. Kosai, V. Liquori, V. Randall, J.P. Rosbeck, S. Sen, P. Wetzel, M.J. Halmos, A. Patrick, A.T. Hunter, J.E. Jensen, T.J. de Lyon, W Johnson, B. Walker, W Trussel, A. Hutchinson, and R.S. Balcerak, "Advances in linear and area HgCdTe APD arrays for eyesafe LADAR sensors", *Proc. SPIE* **4454**, 198–211 (2001).

10. J.D. Beck, C.F. Wan, M.A. Kinch, and J.E. Robinson, "MWIR HgCdTe avalanche photo-diodes", *Proc. SPIE* **4454**, 188–197 (2001).

11. I. Baker, S. Duncan, and J. Copley, "A low-noise, laser-gated imaging system for long-range target identification", *Proc. SPIE* **5406**, 133–144 (2004).

12. I.M. Baker and C.D. Maxey, "Summary of HgCdTe 2D array technology in the UK", *J. Electron. Mater.* **30**, 682 (2003).

13. M.A. Kinch, "HDVIP FPA technology at DRS", *Proc. SPIE* **4369**, 566 (2001).

14. R.S. Hall, N.T. Gordon, J. Giess, J.E. Hails, A. Graham, D.C. Herbert, D.J. Hall, P. Southern, J.W. Cairns, D.J. Lees, and T. Ashley, "Photomultiplication with low excess noise factor in MWIR to optical fiber compatible wavelengths in cooled HgCdTe mesa diodes", *Proc. SPIE* **5783**, 412–423 (2005).

15. S. Horn, P. Norton, K. Carson, R. Eden, and R. Clement, "Vertically-integrated sensor arrays – VISA", *Proc. SPIE* **5406**, 332–340 (2004).

16. R. Balcerak and S. Horn, "Progress in the development of vertically-integrated sensor arrays", *Proc. SPIE* **5783**, 384–391 (2005).

17. Cross-section of the SEM was made by RTI who was teamed with DRS on this task. The photo was provided courtesy of Jim Robinson of DRS.

18. D. Murphy, M. Ray, A. Kennedy, J. Wyles, C. Hewitt, R. Wyles, E. Gordon, T. Sessler, S. Baur, D. Van Lue, S. Anderson, R. Chin, H. Gonzalez, C. Le Pere, S. Ton, and T. Kostrzewa, "Expanded applications for high performance

VO$_x$ microbolometer FPAs", *Proc. SPIE* **5783**, 448–459 (2005).

19. C.J. Han, R. Rawlings, M. Sweeney, S. Whicker, D. Peysha, J.E. Clarke, B. Sullivan, C. Li, and P. Howard, "320×240 and 640×480 UFPAs for TWS and DVE applications", *Proc. SPIE* **5783**, 459–465 (2005).

20. P.W. Norton and M. Kohin, "Technology and application advancements of uncooled imagers", *Proc. SPIE* **5783**, 424–430 (2005).

21. J.J. Yon, A. Astier, S. Bisotto, G. Chamingis, A. Durand, J.L. Martin, E. Mottin, J.L. Ouvrier-Buffet, and J.L. Tissot, "First demonstration of 25- m pitch uncooled amorphous silicon microbolometer IRFPA at LETI-LIR", *Proc. SPIE* **5783**, 432–441 (2005).

22. M. Ueno, Y. Kosasayama, T. Sugino, Y. Nakaki, Y. Fujii, H. Inoue, K. Kama, T. Seto, M. Takeda, M. Kimata, "640×480 pixel uncooled infrared FPA with SOI diode detectors", *Proc. SPIE* **5783**, 566–577, (2005).

23. F.P. Pantuso, "The path to affordable and available 640×480 uncooled FPAs", *Proc. SPIE* **5783**, 439–443 (2005).

24. BAE System data provided by Peter Norton, private communication.

25. Figure of merit also adjusted for pixel size in this case – A^2/25^2.

26. S. Horn, D. Lohrman, P. Norton, K. McCormack, and A. Hutchinson, "Reaching for the sensitivity limits of uncooled and minimally cooled thermal and photon infrared detectors", *Proc. SPIE* **5783**, 401–411 (2005).